VIII International Conference on Computational Methods in Marine Engineering
MARINE 2019
R. Bensow and J. Ringsberg (Eds)

VALIDATION OF A ROLL DECAY TEST OF AN OFFSHORE INSTALLATION VESSEL USING OPENFOAM

MARINE 2019

BRECHT DEVOLDER[*], FLORIAN STEMPINSKI[†], ARJAN MOL[†] AND PIETER RAUWOENS[*]

[*] Department of Civil Engineering, Construction Technology Cluster
KU Leuven, campus Bruges
Spoorwegstraat 12, 8200 Brugge, Belgium
e-mail: brecht.devolder@kuleuven.be, pieter.rauwoens@kuleuven.be

[†] DEME group
Haven 1025, Scheldedijk 30, 2070 Zwijndrecht, Belgium
Email: stempinski.florian@deme-group.com, mol.arjan@deme-group.com

Key words: Numerical modelling; CFD; OpenFOAM; Floating structures

Abstract. In this work, the offshore heavy lift DP2 jack-up vessel Innovation from the DEME group is studied using the Computational Fluid Dynamics (CFD) toolbox OpenFOAM. The two-phase Navier-Stokes fluid solver is coupled with a motion solver using a partitioned fluid-structure interaction algorithm. Firstly, two dimensional numerical simulations of a cross-section of the hull are performed using two different mesh motion techniques: a mesh morphing method and an overset mesh method. Subsequently, the addition of a bilge keel pair on the hull is studied numerically by performing a two dimensional roll decay simulation. Finally, a three dimensional simulation is performed for a roll decay test and validated by using experimental data measured in the MARIN seakeeping and manoeuvring basin. As a first result, the coupled CFD–motion solver proofs to be a promising toolbox for the study of fluid-structure interaction problems of realistic marine structures such as an offshore installation vessel.

1 INTRODUCTION

Floating structures are prominently present in coastal and offshore regions, e.g. ships, pontoons, barges and pipelines. In the future, it is expected that innovative floating structures such as wave energy converters and wind turbines will be installed for renewable energy production. These structures need special installation vessels such as a heavy lift jack-up vessel or a heavy lift floating installation vessel. The workability of these vessels depends on the wave, current and wind loading. Not only the forcing is of large importance for the installation of structures but also the response to the environmental loads needs an accurate quantification.

Nowadays, simplified radiation-diffraction models such as linear potential flow solvers based on boundary element methods (BEM) are used to simulate vessel motions in waves [1,2]. These models are not capable in resolving nonlinear, viscous and turbulent effects and complex free surface deformations such as waves breaking on a vessel. Computational Fluid Dynamics (CFD) is selected to overcome these shortcomings. For example, the roll damping of a vessel

with forward speed is governed by viscous effects. By using a CFD model, the contribution of viscous effects to the roll damping is resolved without any simplification to the underlying physics. As a result, the roll damping coefficient of a vessel can be obtained accurately and can be used as input for simplified models such as BEM to perform a large and wide variety of numerical simulations.

CFD models have been successfully applied and validated for numerous studies related to marine applications such as wave generation [3–5], wave-current generation [6], wave breaking [7,8], wave-structure interaction [9–12] and seakeeping simulations [13–15]. In general for CFD models, a balance has to be sought between numerical accuracy and numerical efficiency to obtain accurate results in an acceptable time window.

In this work, the offshore heavy lift DP2 jack-up vessel Innovation from the DEME group is studied, see Figure 1. The vessel has a length of 147.50 m, a beam of 42 m and a depth of 11 m. It is mainly used for the installation of offshore structures such as offshore wind turbines foundations.

The paper is structured as follows. In section 2, the experimental tests are briefly presented. Section 3 reports the numerical framework used for the simulations presented in section 4. An outlook to further research is listed in section 5 and the conclusions are given in section 6.

Figure 1: The offshore heavy lift DP2 jack-up vessel Innovation (DEME group).

2 EXPERIMENTAL SETUP

The experimental tests used in this work are performed in the seakeeping and manoeuvring basin in MARIN (The Netherlands). The basin measures 170 x 40 x 5 metres in length, width and water depth respectively. The wave generation system comprises of 331 individual flaps of 0.6 m width. At the opposite side, a beach is absorbing the incoming waves. A scale model of the Innovation was built to a geometric scale ratio of 1 to 30, see Figure 2. The key geometrical properties of the vessel are listed in Table 1. The underwater part of the scale model is equipped with four azimuthing stern thrusters, three bow tunnel trusters, four lattice jack-up legs with spudcans, a central skeg and a bilge keel pair. Note that the four lattice legs are not physically present during the model tests but their mass and inertia have been taken into account for the weight distribution by using equivalent masses.

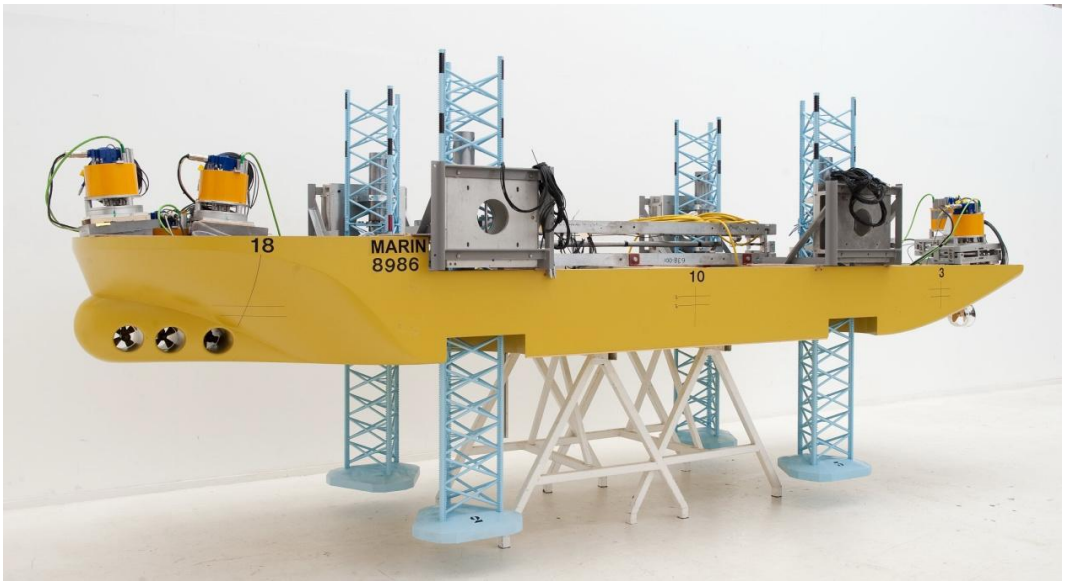

Figure 2: Scale model of the Innovation used for the experimental measurements (scale 1 to 30).

Table 1: Geometrical properties of the Innovation, both for prototype and model scale (1:30).

Parameter	Units	Prototype	Model
Length	m	147.500	4.916
Breadth	m	42.000	1.400
Depth	m	11.000	0.367
Mass *	kg	28 135 800	1 016.650
Draft	m	5.959	0.199
Mass radius of gyration around X-axis	m	21.700	0.723
Mass radius of gyration around Y-axis	m	42.300	1.410
Centre of gravity (X) from aft	m	73.095	2.437
Centre of gravity (Y) from centre line	m	0.000	0.000
Centre of gravity (Z) from keel (KG)	m	17.665	0.589

* Salt water (1025 kg/m³) is assumed in prototype while fresh water (1000 kg/m³) was used for the experiments.

3 NUMERICAL FRAMEWORK

Numerical modelling is performed for the study of a floating offshore installation vessel. The two-phase flow solver with dynamic mesh handling is available in OpenFOAM-v1812 [16,17] to perform transient simulations of a floating structure in a numerical basin. In order to simulate the fluid-structure interaction (FSI) problem, a partitioned approach is used in which a CFD fluid solver (section 3.1) and a motion solver (section 3.2) are called consecutively by a coupling algorithm (section 3.3). Details regarding the mesh motion and boundary conditions are given in sections 3.4 and 3.5 respectively.

3.1 CFD fluid solver

Simulations of the two-phase flow field are performed by solving the incompressible RANS equations and a conservation equation for the Volume of Fluid (VoF) [18] using a finite volume method [19]. Turbulent effects are taken into account by applying a buoyancy-modified *k-ω SST* turbulence model [7,20]. This model is developed to obtain a stable wave propagation model without wave damping due to RANS turbulence modelling. It also predicts the turbulence level inside the flow field more accurately during wave breaking. In particular, a buoyancy-modified turbulence model significantly reduces the overestimation of turbulent kinetic energy in the two-phase flow field, commonly presented in literature for wave simulations using a CFD fluid solver.

For all simulations the following settings are used: first order, bounded, implicit time discretisation; a maximum Courant number of 0.30; upwind discretisation for the turbulent divergence operators; central discretisation for the pressure gradient, the diffusion terms and all the other divergence operators.

3.2 Motion solver

The kinematic motion of a rigid structure is calculated by a six degrees of freedom motion solver. Three translations (surge, sway, heave) and three rotations (roll, pitch and yaw) are allowed. The motion of the structure is based on the overall force F and the torque τ acting on all boundary faces calculated by the fluid solver:

$$\sum F = ma \tag{1}$$

$$\sum \tau = I\alpha \tag{2}$$

in which m is the mass, I is the moment of inertia tensor and a and α the linear and angular acceleration vector. Subsequently, a first order implicit integration scheme is used to obtain the velocity, position, angular velocity and orientation of the rigid structure during every time step of the transient simulation.

3.3 Coupling algorithm

This section presents the coupling algorithm between a CFD fluid solver (section 3.1) and a motion solver (section 3.2). The coupling algorithm is an extension of the developments reported in previous work of the main author [21] based on the IQN-ILS algorithm from [22]. This coupling algorithm results in stable simulations for the case of significant added mass

effects. It will also reduce the number of sub iterations to reach convergence between the flow field around and the motion of the floating structure during every time step of the transient simulation, increasing the computational efficiency. The numerical implementation of the accelerated coupling algorithm is documented in Algorithm 1. $\mathcal{M}$ represents the motion solver, $\mathcal{F}$ the CFD fluid solver and $\mathcal{F} \circ \mathcal{M}$ means that the output of $\mathcal{M}$ is given as input to $\mathcal{F}$. At the start of a FSI simulation, all the variables are initialised, such as the pressure, velocity, volume fraction and turbulent quantities. For each time step, there are $i + 1$ sub iterations needed to reach convergence between the fluid and the motion solver. Note that the algorithm is formulated in terms of a generalised vector x, which is in our case the linear acceleration a as well as the rotational acceleration α (i.e. the algorithm is called twice during every sub iteration). The relative residual has to be smaller than a value ε which is equal to 0.01 for the simulations presented. The relaxation factor ω must be between 0 and 1 and is equal to 0.5 in this paper.

Algorithm 1: Accelerated coupling algorithm used for fluid-structure interaction problems.

$i = 0$
$\tilde{x}^0 = \mathcal{F} \circ \mathcal{M}(x^0)$
$r^0 = \tilde{x}^0 - x^0$
while $\left|r^i\right| / \tilde{x}^i > \varepsilon$ **do**
    if $i = 0$ **then**
        $x^{i+1} = x^i$
    if $i = 1$ **then**
        $x^{i+1} = x^i + \omega r^i$
    else
        $x^{i+1} = x^i + \left[\frac{(\tilde{x}^i - \tilde{x}^{i-1})(r^i - r^{i-1})^T}{(r^i - r^{i-1})^T (r^i - r^{i-1})} - I\right](-r^i)$
        in which I is the unity tensor
    end if
    $\tilde{x}^{i+1} = \mathcal{F} \circ \mathcal{M}(x^{i+1})$
    $r^{i+1} = \tilde{x}^{i+1} - x^{i+1}$
    $i++$
end while

3.4 Mesh motion

In this work, two different mesh motion methods are applied: mesh morphing and overset. The mesh morphing method used within this study is based on spherical linear interpolation (SLERP). The motion of the computational cells is a function of the distance to the moving boundary. The method enforces smoothness and the distance function has a cosine profile to preserve shape of cells close to the moving surface [23]. More recently, the overset method is implemented in the OpenFOAM toolbox to avoid mesh morphing [24]. As a result, undesirable mesh deformation (i.e. high non-orthogonality and skewness of the grid cells) around the air-water interface is absent, reducing the discretisation error for the applied finite volume method. On the other hand, the overset method is interpolating between a background mesh and one or more overset meshes which leads to interpolation errors.

3.5 Boundary conditions

All the simulations presented are performed in a numerical basin which represents the physical basin as good as possible. However, some simplifications are made in order to obtain economical simulation times. For example, the depth of the numerical basin is limited to 1 m instead of 5 m in the experimental facility. Also a reduction of length in the longitudinal direction is made. All these simplifications will however not affect significantly the numerical results presented in this paper.

Each boundary of the computational domain needs specific boundary conditions. The bottom and the four side walls of the basin are set to a no-slip condition and behaves as a fully reflective structure: a Dirichlet boundary condition is set for the velocity (0 m/s in all directions) while the pressure and volume fraction are set to a Neumann condition. The atmospheric conditions at the top of the numerical domain are set to a mixed Dirichlet-Neumann boundary condition for the velocity, pressure and volume fraction. In order to have convergence between the fluid and motion solver, the following kinematic condition needs to be fulfilled at the interface between the fluid and the body:

$$u_{fluid} = u_{body} \tag{3}$$

in which u_{fluid} and u_{body} are the vertical fluid velocity and the vertical body's velocity, respectively. As such, this velocity is used in the moving wall boundary condition at the body's interface.

Wall functions are activated for k and ω on the boundary faces of the floating structure. A continuous wall function based on Spalding's law [25] switching between low- and high-Reynolds numbers is implemented for the turbulent viscosity ν_t. The initial values for k and ω in the computational domain are set to 10^{-10} m²/s² and 1.0 s^{-1} respectively.

4 RESULTS AND DISCUSSION

Firstly, two dimensional (2D) numerical simulations for a roll decay test are performed using two different mesh motion techniques: mesh morphing and overset. Subsequently, the addition of a bilge keel pair is also studied by a 2D roll decay test. Lastly, a full three dimensional (3D) simulation is performed for a roll decay test and validated by using experimental data measured in the MARIN seakeeping and manoeuvring basin. During the roll decay tests presented, the vessel is inclined to an initial roll angle of 2 degrees and is then released. The vessel begins a roll oscillation with a decaying amplitude until all the hydrodynamic forces on the vessel are again in equilibrium with the weight of the vessel. For all the simulations, *snappyHexMesh* has been used for mesh generation.

4.1 2D roll decay test without a bilge keel pair

For the 2D simulations, the midship cross-section of the Innovation is used without the presence of a bilge keel pair. After discretisation, the size of a cell around the hull in *Y*-direction and *Z*-direction is equal to 0.02 m and 0.01 m respectively. The cells are gradually becoming larger towards the boundaries of the computational domain. This will reduce the number of cells and will speed up the simulations without losing accuracy of the roll decay test. In total six simulations for each mesh motion technique (mesh morphing and overset) are performed: without and with boundary layer, and additional local refinements in *Y*- and *Z*-directions around

the hull, see Table 2. An overview of the computational domain is depicted in Figure 3a for the mesh morphing method (case1-SLERP). Figure 3b shows a detail around the cross-section with boundary layer (case1-SLERP+BL).

Table 2: An overview of the 2D roll decay test simulations.

Simulation	Boundary layer	Δ*y* [m]	Δ*z* [m]	# cells	Simulation time [s]	Roll angle [°]
case1-SLERP	✗	0.02	0.01	39 410	715	1.069
case1-overset				49 410	2 721	1.331
case2-SLERP	✗	0.01	0.005	53 242	2 099	1.264
case2-overset				84 840	7 820	1.440
case3-SLERP	✗	0.005	0.0025	80 328	15 113	1.331
case3-overset				168 960	83 062	1.500
case1-SLERP+BL	✓	0.02	0.01	40 052	812	1.164
case1-overset+BL				50 052	3174	1.369
case2-SLERP+BL	✓	0.01	0.005	54 520	2 391	1.275
case2-overset+BL				87 408	10 495	1.478
case3-SLERP+BL	✓	0.005	0.0025	82 872	16 392	1.339
case3-overset+BL				177 126	149 759	1.511

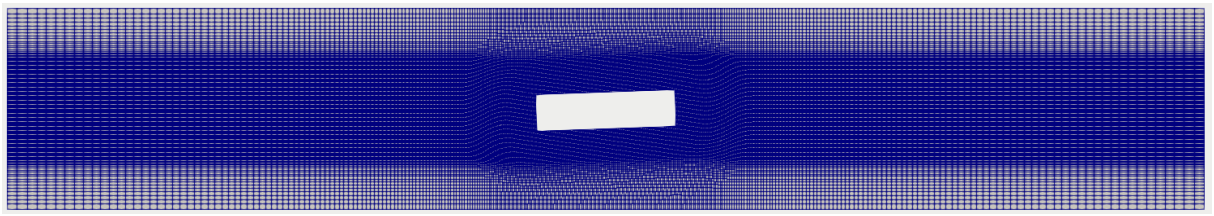

(a)

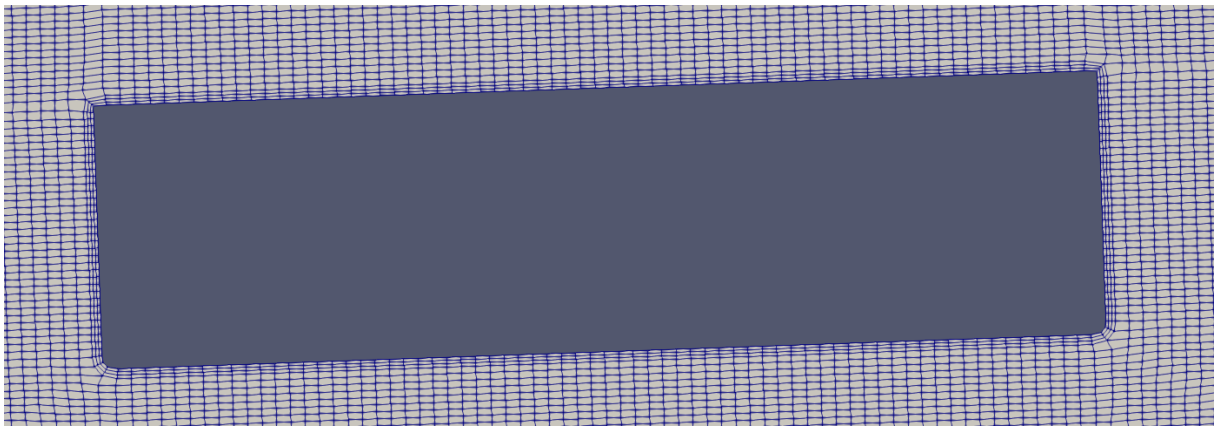

(b)

Figure 3: Computational domain in 2D, (a) full domain, (b) boundary layer around the hull.

The numerical results of the roll decay test with an initial roll angle of 2 degrees are presented in Figure 4a and Figure 4b using the SLERP and overset approach respectively. The roll angle is given as a function of time. After 7 seconds, the roll motion is almost fully damped out. The value of the roll angle at the first peak around 1.5 seconds is also reported in the last column of Table 2. The solutions are converging monotonically for each additional local refinement, both without and with boundary layer. The presence of a boundary layer near the hull is not influencing the results significantly, both for the SLERP and overset approach. Between two levels of refinement, the difference in roll angle around 1.5 seconds is smaller for the overset method than for the SLERP approach. In addition, the difference between SLERP and overset is decreasing for an increase in the number of cells due to local refinements. It is very important to stress that the overset method requires a significantly larger amount of computational time, see Table 2. This is not only related to the larger number of computational cells but also due to the implementation of the overset interpolation operation.

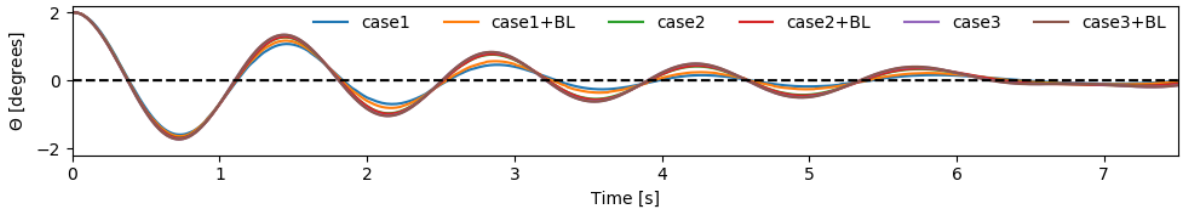

(a)

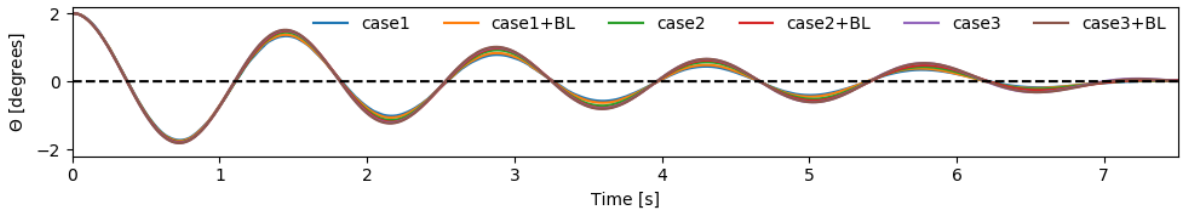

(b)

Figure 4: Roll angle as a function of time during a roll decay test: (a) SLERP (b) overset.

4.2 2D roll decay test with a bilge keel pair

In this section a bilge keel pair is added to the hull of the vessel. During the 3D model tests, a bilge keel pair was installed in order to enhance the roll stability of the vessel. Local refinement of the computational cells (case1-SLERP) is required to create a proper mesh around the bilge keel, see Figure 5. The numerical results are presented in Figure 6 for a simulation without and with bilge keel. It is demonstrated that the addition of a bilge keel pair only leads to a small increase of the roll damping. Also the natural roll period is slightly increasing if a bilge keel pair is modelled. Figure 7 shows the velocity field around the cross-section. By adding a bilge keel pair, the local velocity magnitude of the water increases significantly which affects slightly the roll motion as well. Interestingly, the simulation without bilge keel pair was completed in 1 360 seconds while with a bilge keel pair 2 388 seconds were needed. This increase is originating from the limiting Courant number and smaller cells near the bilge keels.

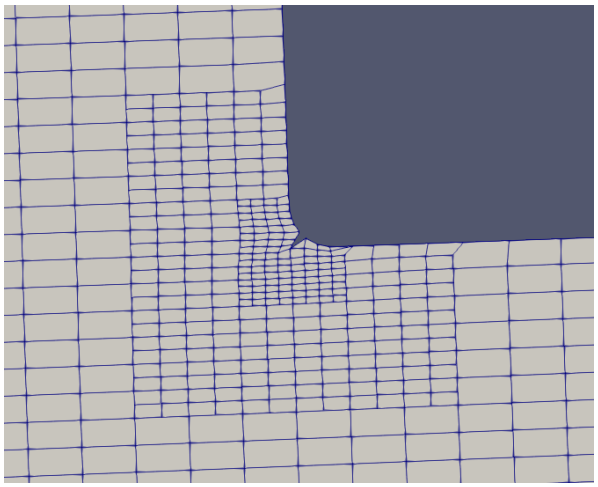

Figure 5: Detail of the computational domain (2D) around the cross-section of the hull with a bilge keel pair.

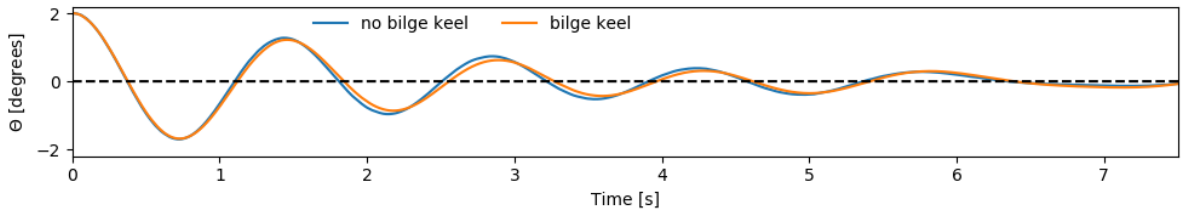

Figure 6: Roll angle as a function of time during a roll decay test: without and with bilge keel pair.

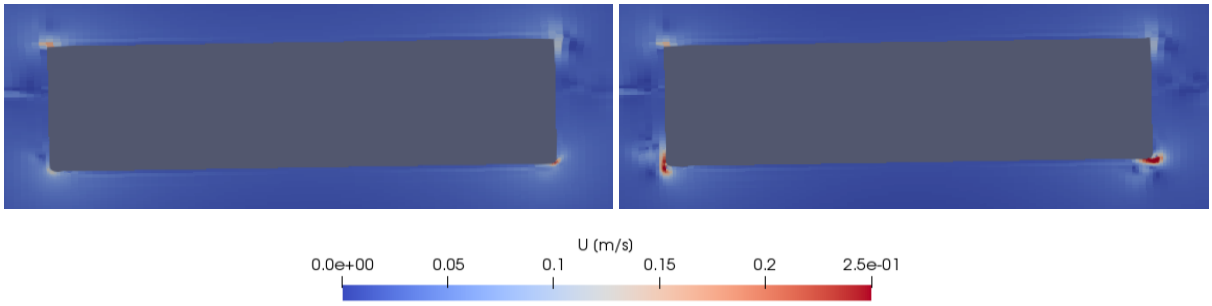

Figure 7: Velocity field around the hull: (left) without bilge keel pair, (right) with bilge keel pair.

4.3 3D roll decay test

In this section, a 3D simulation of a roll decay test with zero forward speed is performed and validated with the experimental measurements introduced in section 2. The computational domain around the hull is depicted in Figure 8. Local refinements are made around the hull and the free water surface were the mesh motion is happening (SLERP interpolation). The overset method is not chosen due to the larger computational overhead (see section 4.1 for the 2D simulations). In addition, the bilge keel is not considered in a first instance due to the limiting effect and large increase in computational time (see section 4.2). The final mesh consists of 672 316 cells and has a resolution of 0.40 m in the far field down to 0.05 m near the hull.

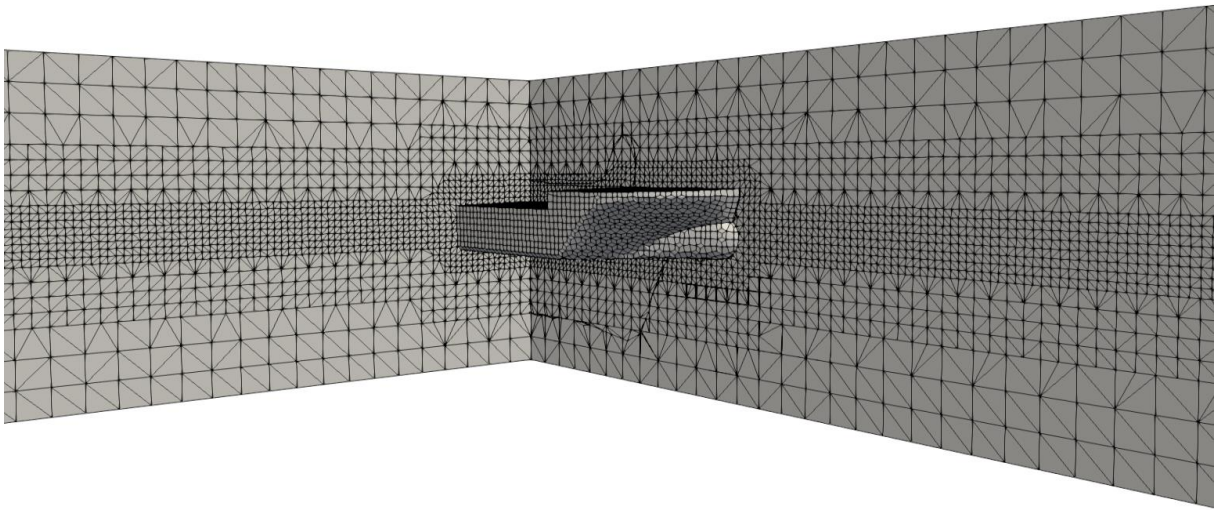

Figure 8: Computational domain around the hull of the Innovation. Two vertical cross-sections are shown to indicate the discretisation in the numerical basin.

The numerical and experimental results of the roll decay test are given as time series in Figure 9. In general, the roll damping motion predicted by the numerical model is in a very good agreement with the experimental measurements. However after 10 seconds, the observed roll damping is slightly bigger for the experimental result signal compared to the numerical result. These differences are addressed to the simplifications made to the geometry used for the numerical simulations. For example, during the experimental propulsion tests, the spudcans were not fully hidden inside their garages increasing the resistance. This might also add damping during the experimental roll decay tests compared to the numerical simulations in which the spudcans are not considered at all on the geometry. Also the propellers installed on the ship model are excluded on the numerical geometry. As reported by [26], the eddy damping and wave radiation damping have a significant contribution to the total roll damping for a vessel with zero forward speed. Both of them depend on the position of the centre of gravity and the shape of the hull.

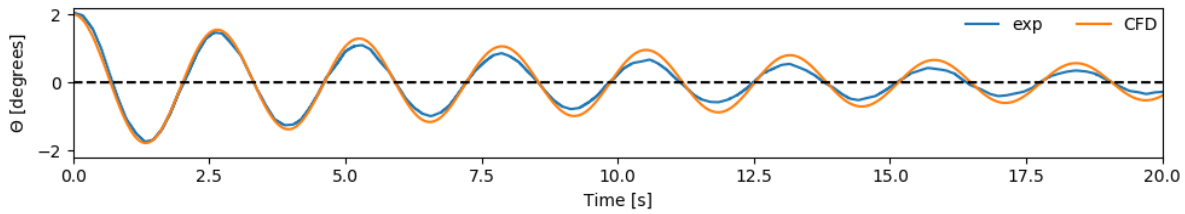

Figure 9: Roll angle as a function of time during a roll decay test of an offshore installation vessel: numerical CFD result and experimental measurement.

5. RESEARCH TOPICS UNDER INVESTIGATION

The topics listed below will be investigated in the near feature:

- Validation of roll damping simulations of a vessel with a forward speed;
- Overset mesh method for seakeeping simulations;
- Roll damping tests of the Innovation on which spudcan shoes are installed;
- Validation of a freely floating vessel in regular waves.

6 CONCLUSIONS

We have presented numerical simulations of a vessel during a roll decay test. Two mesh motion techniques have been compared using 2D simulations: SLERP and overset. In addition, the addition of a bilge keel pair is studied which has only a small influence on the roll damping motion. A 3D simulation of an offshore installation vessel, the Innovation from the DEME group, during a roll decay test with zero forward speed is validated by using experimental data. Discrepancies have been observed, discussed and further research is proposed to fully understand the hydrodynamics around the vessel during seakeeping simulations.

7 ACKNOWLEDGEMENTS

The first author is postdoctoral researcher at the department of civil engineering at KU Leuven, campus Bruges. The project is a collaboration between KU Leuven and DEME and is funded by the agency Flanders Innovation & Entrepreneurship (VLAIO) and DEME.

REFERENCES

[1] Babarit A, Delhommeau G. Theoretical and numerical aspects of the open source BEM solver NEMOH. Proc. 11th Eur. Wave Tidal Energy Conf., 2015.

[2] ANSYS. ANSYS Aqwa n.d.

[3] Jacobsen NG, Fuhrman DR, Fredsøe J. A wave generation toolbox for the open-source CFD library: OpenFoam®. Int J Numer Methods Fluids 2012;70:1073–88. doi:10.1002/fld.2726.

[4] Higuera P, Lara JL, Losada IJ. Realistic wave generation and active wave absorption for Navier-Stokes models. Application to OpenFOAM. Coast Eng 2013;71:102–18. doi:10.1016/j.coastaleng.2012.07.002.

[5] Windt C, Davidson J, Schmitt P, Ringwood J V., Windt C, Davidson J, et al. On the Assessment of Numerical Wave Makers in CFD Simulations. J Mar Sci Eng 2019, Vol 7, Page 47 2019;7:47. doi:10.3390/JMSE7020047.

[6] Lara JL, Barajas G, Maza M, Losada IJ. Wave-current generation with OpenFOAM. Application to coastal and offshore structures. 4th OpenFOAM User Conf., Cologne, Germany: 2016.

[7] Devolder B, Troch P, Rauwoens P. Performance of a buoyancy-modified k-ω and k-ω SST turbulence model for simulating wave breaking under regular waves using OpenFOAM®. Coast Eng 2018;138:49–65. doi:10.1016/j.coastaleng.2018.04.011.

[8] Larsen BE, Fuhrman DR. On the over-production of turbulence beneath surface waves in Reynolds-averaged Navier–Stokes models. J Fluid Mech 2018;853:419–60. doi:10.1017/jfm.2018.577.

[9] Devolder B, Stratigaki V, Troch P, Rauwoens P. CFD Simulations of Floating Point Absorber Wave Energy Converter Arrays Subjected to Regular Waves. Energies 2018;11:641. doi:10.3390/en11030641.
[10] Higuera P, Liu PL-F, Lin C, Wong W-Y, Kao M-J. Laboratory-scale swash flows generated by a non-breaking solitary wave on a steep slope. J Fluid Mech 2018;847:186–227. doi:10.1017/jfm.2018.321.
[11] Windt C, Davidson J, Akram B, Ringwood J V. Performance assessment of the overset grid method for numerical wave tank experiments in the OpenFOAM environment. Proc. ASME 2018 37th Int. Conf. Ocean. Offshore Arct. Eng., 2018, p. 1–10.
[12] Di Paolo B, Lara JL, Barajas G, Paci A, Losada IJ. Numerical Analysis of Wave and Current Interaction With Moored Floating Bodies Using Overset Method. Proc. ASME 2018 37th Int. Conf. Ocean. Offshore Arct. Eng., ASME; 2018, p. 1–10. doi:10.1115/OMAE2018-77284.
[13] Piehl HP. Ship Roll Damping Analysis. University of Duisburg-Essen, 2016.
[14] Gatin I, Vukčević V, Jasak H, Rusche H. Enhanced coupling of solid body motion and fluid flow in finite volume framework. Ocean Eng 2017;143:295–304. doi:10.1016/j.oceaneng.2017.08.009.
[15] Gatin I, Vukčević V, Jasak H, Seo J, Rhee SH. CFD verification and validation of green sea loads. Ocean Eng 2018;148:500–15. doi:10.1016/j.oceaneng.2017.10.026.
[16] Weller HG, Tabor G, Jasak H, Fureby C. A tensorial approach to computational continuum mechanics using object-oriented techniques. Comput Phys 1998;12:620. doi:10.1063/1.168744.
[17] OpenCFD. OpenFOAM 2018. https://www.openfoam.com/.
[18] Berberović E, van Hinsberg NP, Jakirlić S, Roisman I V., Tropea C. Drop impact onto a liquid layer of finite thickness: Dynamics of the cavity evolution. Phys Rev E 2009;79:036306. doi:10.1103/PhysRevE.79.036306.
[19] Versteeg HK, Malalasekera W. An Introduction to Computational Fluid Dynamics - The Finite Volume Method. Pearson Education; 2007. doi:10.2514/1.22547.
[20] Devolder B, Rauwoens P, Troch P. Application of a buoyancy-modified k-ω SST turbulence model to simulate wave run-up around a monopile subjected to regular waves using OpenFOAM®. Coast Eng 2017;125:81–94. doi:10.1016/j.coastaleng.2017.04.004.
[21] Devolder B, Troch P, Rauwoens P. Accelerated numerical simulations of a heaving floating body by coupling a motion solver with a two-phase fluid solver. Comput Math with Appl 2018. doi:10.1016/j.camwa.2018.08.064.
[22] Degroote J. Partitioned Simulation of Fluid-Structure Interaction. Arch Comput Methods Eng 2013;20:185–238. doi:10.1007/s11831-013-9085-5.
[23] OpenFOAM Foundation. OpenFOAM 2018. https://openfoam.org/.
[24] Janssens M. Native overset meshes in OpenFOAM. 4th OpenFOAM User Conf. 2016, Cologne, Germany: 2016.
[25] Spalding DB. A Single Formula for the “Law of the Wall.” J Appl Mech 1961;28:455. doi:10.1115/1.3641728.
[26] Himeno Y. Prediction of Ship Roll Damping - State of the Art. Rep Dep Nav Archit Mar Eng Univ Michigan 1981;239.